Experimental Validation of a Metasurface Luneburg Lens Antenna Implemented With Glide-Symmetric Substrate-Integrated Holes

Oskar Zetterstrom, *Student Member, IEEE*, Ramez Hamarneh, and Oscar Quevedo-Teruel, *Senior Member, IEEE*

***Abstract*—In this letter, we present the experimental validation of a K_a-band Luneburg lens antenna based on a novel cost-effective metasurface. The metasurface is composed of a parallel plate waveguide (PPW) loaded with quasi-periodic inclusions in both conductors. The inclusions are square holes printed on a substrate, with vias placed around the holes. The vias connect the printed layer of the substrate to the ground. This configuration is named substrate-integrated hole (SIH). It is demonstrated that the SIH metasurface can obtain a higher effective refractive index, compared to the conventional holey metasurface. To further increase the effective refractive index, the SIHs in the two conductors of the PPW are glide-symmetrically arranged. The refractive index distribution of the Luneburg lens is realized by locally tuning the dimensions of the SIHs. The lens is fed with 11 waveguide feeds with an angular separation of 10°. Thus, the antenna can steer its radiation in a 100° angular range. A flare is integrated with the PPW to match the antenna to the free-space impedance. Since the wave propagates mainly in the PPW air gap, the dielectric losses are low. The measured radiation efficiency of the antenna is roughly 80%.**

***Index Terms*—Glide symmetry, Luneburg lens antenna, substrate-integrated hole (SIH).**

I. Introduction

THE requirements for high data rate and short delays in the new wireless networks can be satisfied using a high operation frequency [1]. Specifically, the frequencies around 28 GHz have received significant attention for the future generations of the mobile communication networks [2].

At these frequencies, the losses in free-space propagation and materials are high, which makes the design of efficient antennas challenging. The propagation losses can be mitigated using high-gain antennas, which often require beam steering of the narrow beam to provide enough coverage. Array antennas can produce a steerable directive beam. However, the feeding networks of arrays become complex and lossy at high frequencies [3]. Alternatively, quasi-optical beamformers such as lenses can produce a steerable high-gain beam without a complex feeding network [4]. One particularly interesting solution is the Luneburg lens [5].

Two-dimensional Luneburg lenses are compact and support one-dimensional beam steering [6]. The gradual refractive index distribution in these lenses can be implemented using dielectrics [7], [8], or mimicked with geodesic surfaces [9]–[11] or metasurfaces [12]–[19]. At millimeter-wave frequencies, the losses in dielectrics are high, so fully metallic configurations are preferred [20]. Therefore, geodesic surfaces or fully metallic metasurfaces have been proposed, since they have low losses.

In a geodesic Luneburg lens, the gradual refractive index is mimicked with a profiled surface [9]. The wide scan range and high efficiency of geodesic Luneburg lens antennas have been demonstrated at K_a-band [10], [11]. Since the profiled surface is smooth, this type of antenna can be cost-effectively manufactured. However, the profiled surface increases the height of the antenna.

In metasurface Luneburg lenses, the gradual refractive index is realized with a quasi-periodic structure. Oppositely to geodesic lenses, metasurface lenses can be fully planar. The refractive index distribution is realized by locally tuning the dimensions of the quasi-periodic structure. The metasurface is typically implemented in a parallel plate waveguide (PPW) configuration and realized using printed circuit board (PCB) technology or milling techniques. In [13], a cost-effective Luneburg lens antenna was designed in a PCB. A wide bandwidth ($\approx 40\%$) is obtained. However, in this design, the waves are mainly confined inside a dielectric, which results in high losses at high frequency. Fully metallic metasurface Luneburg lens antennas were presented in [16]–[19] and a radiation efficiency of 88% was demonstrated [16]. However, these metasurfaces must be milled, which results in a high cost.

The simulated performance of an efficient Luneburg lens antenna suitable for mass-production was presented in [21]. The proposed antenna is based on the substrate-integrated-holes (SIHs) metasurface. The SIH metasurface is integrated in the conductors of a PPW and can be manufactured using conventional PCB techniques. In the SIH structure, the electromagnetic waves propagate mainly in the PPW air gap, which results in low losses. In the present letter, we provide an experimental validation of the Luneburg lens based on the glide-symmetric SIHs presented in [21].

Manuscript received November 25, 2020; revised January 20, 2021; accepted February 8, 2021. Date of publication February 18, 2021; date of current version May 5, 2021. This work was supported by the Strategic Innovation Program Smarter Electronics System—A joint venture of Vinnova, Formas, and the Swedish Energy Agency, under Project High-Int (2019-02103). *(Corresponding author: Oskar Zetterstrom.)*

The authors are with the Division of Electromagnetic Engineering, KTH Royal Institute of Technology, 11428 Stockholm, Sweden (e-mail: oskarz@kth.se; hamarnehramez@hotmail.com; oscarqt@kth.se).

Digital Object Identifier 10.1109/LAWP.2021.3060283

II. Luneburg Lens Antenna Based on Glide-Symmetric SIHs

A Luneburg lens is a rotationally symmetric graded index lens that transforms a spherical/cylindrical wave at the periphery of the lens to a quasi-planar wave in the diametrically opposite direction of the lens [5]. The refractive index distribution varies gradually from $\sqrt{2}$ in the center to 1 at the border of the lens. Consequently, no reflections occur at the interface of the lens and the surrounding media. Additionally, due to the rotational symmetry, beams in different directions are produced by feeding the lens from different positions along the periphery. This enables beam steering without scan losses and a complex feeding network.

The Luneburg lens in [21] is implemented in a PPW configuration. The required refractive index distribution is realized by periodically loading the two conductors of the PPW with glide-symmetric SIHs.

A periodic structure possesses glide symmetry if it is invariant under a translation and a reflection. The electromagnetic properties of periodic structures with glide symmetry was initially studied in the 1960s and 1970s [22]–[25]. In these studies, qualitative dispersion properties of glide-symmetric structures were derived and applied to the design of leaky-wave antennas [24]. Recently, glide-symmetric structures received renewed attention, and quantitative dispersion properties were presented with the help of modern simulation tools. Importantly, it has been demonstrated that glide-symmetric structures provide a higher and less dispersive effective refractive index, compared to their nonglide counterpart [15], [26]–[28]. These properties have been used in the design of microwave lenses [16], [18], [21], [28]–[32].

The refractive index of the Luneburg lens is difficult to reach using holey metasurfaces due to the required small air gap between the two conductors of the PPW. In [16], the effective refractive index of the glide-symmetric holey metasurface is increased by loading the holes with a pin. This results in an increased manufacturing cost and decreased robustness. Alternatively, the holes can be filled with a dielectric, as presented in [33]. To facilitate the manufacturing of the dielectric-filled holey structure, the SIH structure was proposed in [34]. In the SIH structure, the lateral walls of the holes are replaced with an array of vias. The SIH structure can be manufactured using standard PCB techniques and is, thus, suitable for mass production. The unit cells of the dielectric-filled holes and SIHs structures are illustrated in Fig. 1(a) and (b). Due to the dense via placement, vias are shared between adjacent unit cells in the SIH structure.

In Fig. 1(c), the effective refractive indices as a function of frequency for the dielectric-filled holey (dot-dashed lines) and the SIH (solid lines) structures are presented for different values of the hole size s. The remaining dimensions are: $p = 2.7$ mm, $g = 0.6$ mm, $h = 1.575$ mm, $d = 0.3$ mm, and $v = 0.54$ mm. The substrate is RO5870 ($\varepsilon_r = 2.33$ and $\tan\delta = 0.0012$). The SIH structure provide a higher and more dispersive effective refractive index, compared to the dielectric-filled holey structure with the same dimensions. The difference

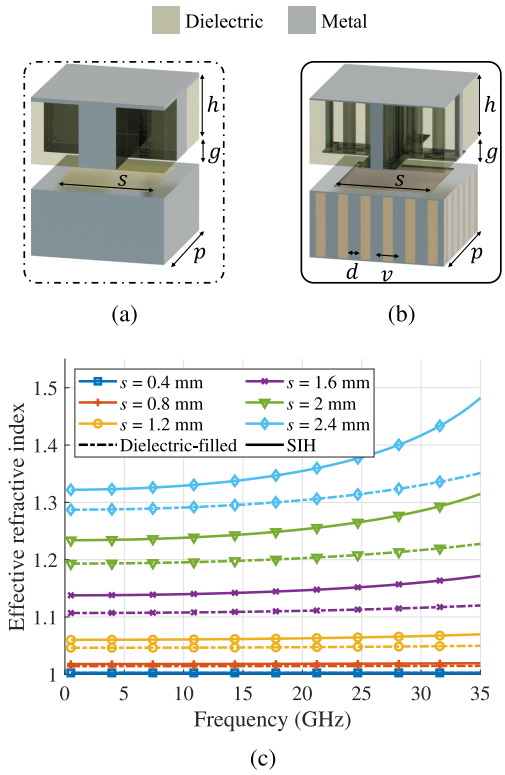

Fig. 1. Comparison of the effective refractive index between the dielectric-filled holey and substrate-integrated-holes structures. Simulated structures: (a) Dielectric-filled holey. (b) Substrate-integrated holes. (c) Effective refractive index for different s. The remaining dimensions are: $p = 2.7$ mm, $g = 0.6$ mm, $h = 1.575$ mm, $d = 0.3$ mm, and $v = 0.54$ mm. The substrate is RO5870 ($\varepsilon_r = 2.33$ and $\tan\delta = 0.0012$). The dot-dashed and solid lines correspond to the dielectric-filled holey and SIH structures, respectively.

in the response of the two structures is due to the different modes that are supported by the cavities. The cavities in the dielectric-filled holey structure form vertical dielectric-filled square waveguides that supports TE and TM modes. These modes have a cut-off frequency higher than the operating frequency of the antenna. Therefore, these modes are evanescent and the depth of the holes h has limited impact on the response [35]. On the other hand, the cavities in the SIH structure form vertical multiconductor waveguides that support propagating modes. Therefore, the response of the SIH structure is affected by the depth of the holes [36].

In Fig. 2, the effective refractive index of the SIH structure at 30 GHz as a function of the hole size s. The remaining dimensions are the same as above. The refractive index of the Luneburg lens can be readily achieved with a gap g of 0.6 mm. This gap is twice as large as the gap in [16], which alleviates the manufacturing.

The refractive index map in Fig. 2 is used to design a Luneburg lens antenna. Each PCB is placed in a metallic casing, as illustrated in Fig. 3. The PCBs are glued to the casings and holes are placed underneath the PCBs to allow for residual glue to escape. The lens is fed with 11 waveguide feeds separated by 10° that are integrated in the metallic casing. Additionally, the metallic casing is terminated in a flare to match the impedance of the

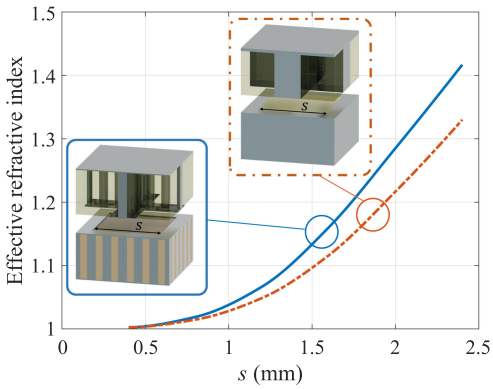

Fig. 2. Effective refractive index of the dielectric-filled and SIH structures at 30 GHz. The dimensions are the same as in Fig. 1.

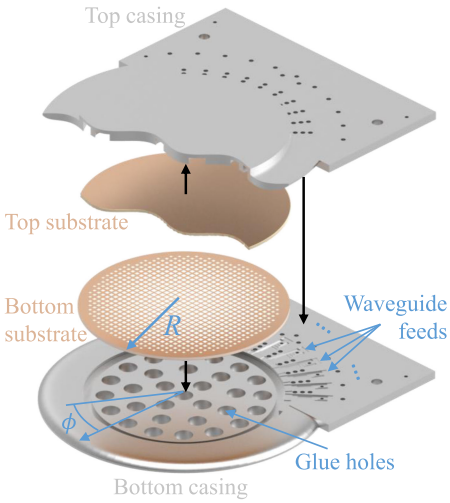

Fig. 3. Illustration of the assembly of the lens antenna. The PCBs are placed in a metallic casing. In total, 11 waveguide feeds are incorporated in the casing and the casing is terminated in a flare. Details on the design of the waveguide feeds and flare are presented in [21].

PPW to the free-space impedance. The design of the flare and feeding waveguides is detailed in [21].

III. Simulation and Measurement Results

The antenna is simulated using the *time-domain solver* of CST Microwave Studio [37]. The simulated normalized electric field distribution at 28 GHz when exciting three different ports is presented in Fig. 4. The lens transforms the cylindrical wave from the feed into a quasi-planar wave at the opposite side of the lens.

The manufactured prototype is presented in Fig. 5. The simulated and measured reflection coefficient is presented in Fig. 6, and the results agree well between 27 and 30 GHz, where a reflection coefficient less than −15 dB is obtained. The higher reflection coefficient in the measured prototype between 24.5 and 27 GHz is believed to be caused by a systematic error in the manufacturing of the feed elements. This discrepancy is expected to be solved with an alternative feed design.

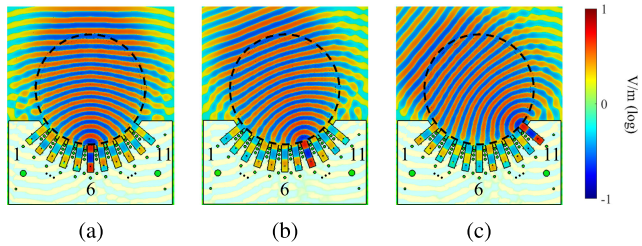

Fig. 4. Normalized electric field distribution in the lens antenna at 28 GHz when exciting waveguides: (a) 6, (b) 8, and (c) 11. The lens is outlined with the black circle and the radius is $R = 55$ mm.

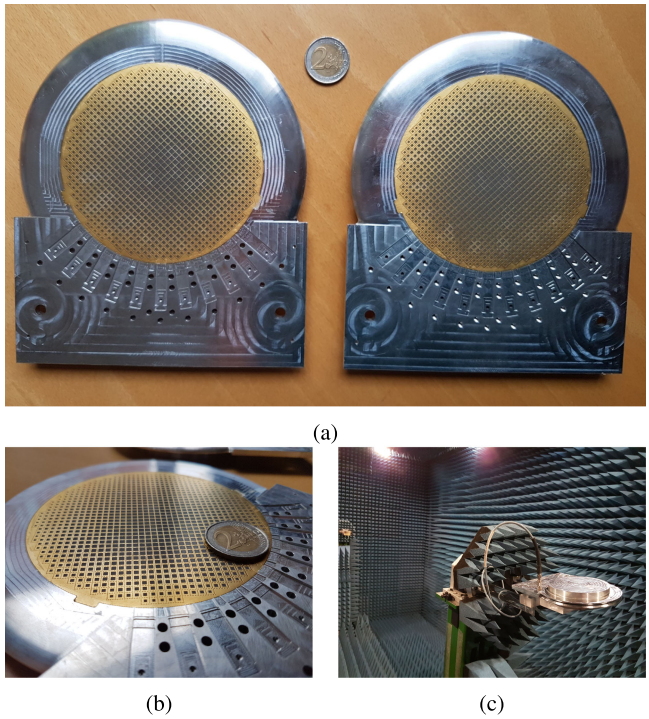

Fig. 5. (a) Top and bottom parts of the manufactured prototype. (b) Close-up view of the bottom part. A 2€ coin is included for size-reference. (c) Measurement setup for the far-field measurement.

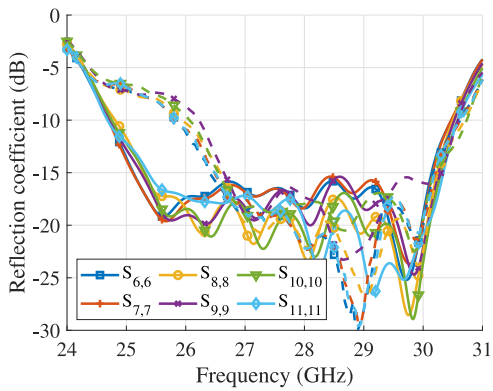

Fig. 6. Simulated (solid lines) and measured (dashed lines) reflection coefficient. The port numbers are indicated in Fig. 4.

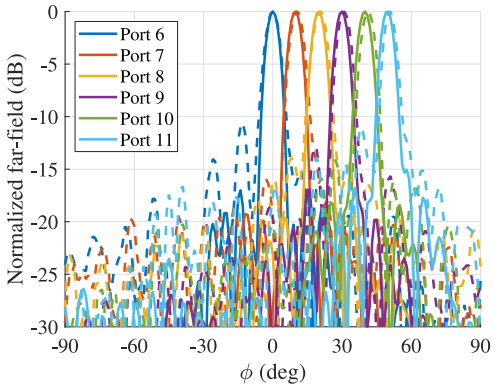

Fig. 7. Simulated (solid lines) and measured (dashed lines) normalized H-plane far field at 28 GHz.

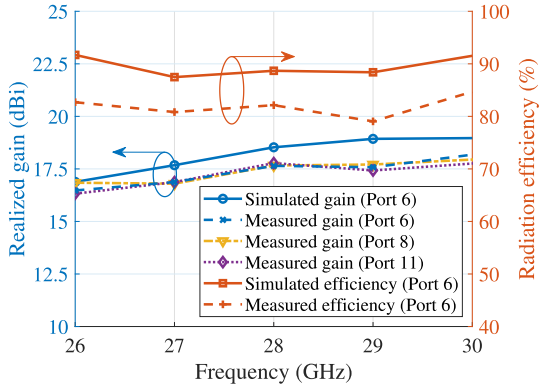

Fig. 9. Simulated and measured efficiency and peak gain.

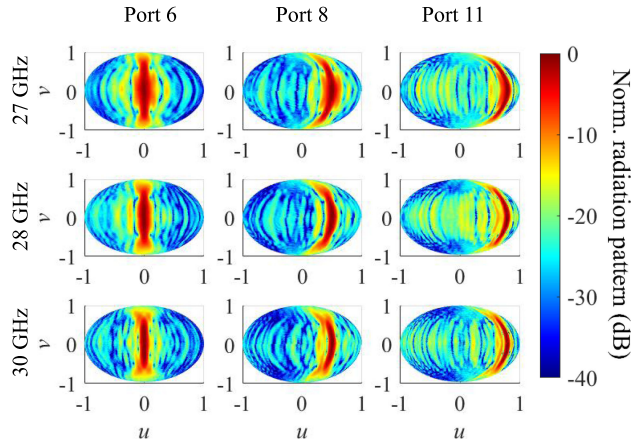

Fig. 8. Measured two-dimensional normalized radiation pattern for waveguide ports 6, 8, and 11 at 27, 28, and 30 GHz.

TABLE I
COMPARISON WITH EXISTING LUNEBURG LENS DESIGNS

Ref.	Freq. (GHz)	Eff. (%)	Printed technology
[13]	9-13	≈ 55	Yes
[16]	25-31	≈ 88	No
[17]	27-39	≈ 88	No
[18]	14-22	-	No
[19]	26-40	≈ 90	No
This work	26-30	≈ 80	Yes

The simulated and measured normalized H-plane far field at 28 GHz is presented in Fig. 7. The results agree well, except for slightly increased beamwidth and side lobes in the measured prototype. The simulated and measured side-lobe level are below -15 and -11 dB for all scan angles. The measured 2-D normalized radiation pattern at 27, 28, and 30 GHz is presented in Fig. 8, for waveguide ports 6, 8, and 11. The antenna produces a fan beam that is stable with frequency and can be scanned in a wide angular range. In Fig. 9, the simulated and measured efficiency and gain are presented. The gain is stable for the different ports, which demonstrates the low scan losses in the antenna. The measured gain is roughly 1 dB lower than the simulated gain. The gain reduction is due to the reduced directivity and increased losses in the manufactured prototype. The reduction in directivity is attributed to manufacturing tolerances of the casings and PCBs, and is roughly 0.5 dB for port 6. The increased losses are attributed to higher metallic (due to higher surface roughness) and dielectric losses than those assumed in the simulations. A better agreement between the simulated and measured result is expected if the surface roughness of the metallic parts is included in the simulations. The measured radiation efficiency is roughly 80% throughout the band.

Table I compare the presented antenna with existing Luneburg lens antenna designs in the literature. It is observed that the presented design has a similar efficiency as the fully metallic designs [16]–[19] that requires a more expensive manufacturing at this frequency range. Furthermore, despite operating at higher frequency, the presented antenna obtains a higher efficiency than the existing design in printed technology [13].

IV. CONCLUSION

In this letter, we present the experimental validation of an efficient K_a-band Luneburg lens antenna suitable for mass production. The antenna is based on the SIH metasurface, which consists of an array of cavities loaded into the two conductors of a PPW. The cavities are formed by printing squares on a substrate. The squares are surrounded by vias that connect the printed layer to the ground. The presence of the dielectric inside the cavities results in an increased effective refractive index of the metasurface, compared to the metasurface with empty cavities. However, since the waves are mainly propagating in the PPW air gap, the losses are low. To increase the effective refractive index of the metasurface, the cavities in the two conductors of the PPW are glide-symmetrically arranged. With the proposed structure, the refractive index of the Luneburg lens can be obtained with twice the PPW air gap, compared to the previously reported holey structures [16]. This larger air gap alleviates the manufacturing. The lens is fed with 11 waveguide feeds and the PPW is terminated in a flare. The measured results demonstrates that the antenna can scan a directive fan beam in a 100° range in the H-plane. The measured radiation efficiency is roughly 80%.

REFERENCES

[1] Y. Wang, J. Li, L. Huang, Y. Jing, A. Georgakopoulos, and P. Demestichas, "5G mobile: Spectrum broadening to higher-frequency bands to support high data rates," *IEEE Veh. Technol. Mag.*, vol. 9, no. 3, pp. 39–46, Sep. 2014.

[2] G. Sellin, and M. Edberg, "Ericsson microwave outlook," Oct. 2020, Accessed: Nov. 16, 2020. [Online]. Available: https://www.ericsson.com/4a811d/assets/local/reports-papers/microwave-outlook/2020/2020-ericsson-microwave-outlook-report-digital.pdf

[3] R. Garg and A. S. Natarajan, "A 28-GHz low-power phased-array receiver front-end with 360° RTPS phase shift range," *IEEE Trans. Microw. Theory Techn.*, vol. 65, no. 11, pp. 4703–4714, Nov. 2017.

[4] O. Quevedo-Teruel, M. Ebrahimpouri, and F. Ghasemifard, "Lens antennas for 5G communications systems," *IEEE Commun. Mag.*, vol. 56, no. 7, pp. 36–41, Jul. 2018.

[5] R. Luneburg, *Mathematical Theory of Optics*. Providence, RI, USA: Brown Univ. Press, 1944, pp. 208–213.

[6] G. Peeler and D. Archer, "A two-dimensional microwave Luneberg lens," *IEEE Trans. Antennas Propag.*, vol. AP-1, no. 1, pp. 12–23, Jul. 1953.

[7] L. Xue and V. F. Fusco, "24 GHz automotive radar planar Luneburg lens," *Microw., Antennas Propag.*, vol. 1, no. 3, pp. 624–628, Jun. 2007.

[8] P. Liu *et al.*, "A novel e-plane-focused cylindrical Luneburg lens loaded with metal grids for sidelobe level reduction," *IEEE Trans. Antennas Propag.*, vol. 68, no. 2, pp. 736–744, Feb. 2020.

[9] K. Kunz, "Propagation of microwaves between a parallel pair of doubly curved conducting surfaces," *J. Appl. Phys.*, vol. 25, no. 5, pp. 642–653, 1954.

[10] Q. Liao, N. Fonseca, and O. Quevedo-Teruel, "Compact multibeam fully metallic geodesic Luneburg lens antenna based on non-Euclidean transformation optics," *IEEE Trans. Antennas Propag.*, vol. 66, no. 12, pp. 7383–7388, Dec. 2018.

[11] N. J. G. Fonseca, Q. Liao, and O. Quevedo-Teruel, "Equivalent planar lens ray-tracing model to design modulated geodesic lenses using non-Euclidian transformation optics," *IEEE Trans. Antennas Propag.*, vol. 68, no. 5, pp. 3410–3422, May 2020.

[12] L. Xue and V. F. Fusco, "Printed holey plate Luneburg lens," *Microw. Opt. Technol. Lett.*, vol. 50, no. 2, pp. 378–380, Dec. 2008.

[13] C. Pfeiffer and A. Grbic, "A printed, broadband Luneburg lens antenna," *IEEE Trans. Antennas Propag.*, vol. 58, no. 9, pp. 3055–3059, Sep. 2010.

[14] S. Maci, G. Minatti, M. Casaletti, and M. Bosiljevac, "Metasurfing: Addressing waves on impenetrable metasurfaces," *IEEE Antennas Wireless Propag. Lett.*, vol. 10, pp. 1499–1502, 2011.

[15] O. Quevedo-Teruel, M. Ebrahimpouri, and M. N. M. Kehn, "Ultrawideband metasurface lenses based on off-shifted opposite layers," *IEEE Antennas Wireless Propag. Lett.*, vol. 15, pp. 484–487, 2016.

[16] O. Quevedo-Teruel, J. Miao, M. Mattsson, A. Algaba-Brazalez, M. Johansson, and L. Manholm, "Glide-symmetric fully metallic Luneburg lens for 5G communications at Ka-band," *IEEE Antennas Wireless Propag. Lett.*, vol. 17, no. 9, pp. 1588–1592, Sep. 2018.

[17] H. Lu, Z. Liu, J. Liu, G. Wu, Y. Liu, and X. Lv, "Fully metallic anisotropic lens crossover-in-antenna based on parallel plate waveguide loaded with uniform posts," *IEEE Trans. Antennas Propag.*, vol. 68, no. 7, pp. 5061–5070, Jul. 2020.

[18] F. Fan, M. Cai, J. Zhang, Z. Yan, and J. Wu, "Wideband low-profile Luneburg lens based on a glide-symmetric metasurface," *IEEE Access*, vol. 8, pp. 85698–85705, 2020.

[19] H. Lu, Z. Liu, Y. Liu, H. Ni, and X. Lv, "Compact air-filled Luneburg lens antennas based on almost-parallel plate waveguide loaded with equal-sized metallic posts," *IEEE Trans. Antennas Propag.*, vol. 67, no. 11, pp. 6829–6838, Nov. 2019.

[20] D. González-Ovejero, N. Chahat, R. Sauleau, G. Chattopadhyay, S. Maci, and M. Ettorre, "Additive manufactured metal-only modulated metasurface antennas," *IEEE Trans. Antennas Propag.*, vol. 66, no. 11, pp. 6106–6114, Nov. 2018.

[21] R. Hamarneh, O. Zetterstrom, and O. Quevedo-Teruel, "Glide-symmetric Luneburg lens using substrate-integrated-holes for 5G communications at ka-band," in *Proc. 14th Eur. Conf. Antennas Propag.*, 2020, pp. 1–5.

[22] P. J. Crepeau and P. R. McIsaac, "Consequences of symmetry in periodic structures," *Proc. IEEE*, vol. 52, no. 1, pp. 33–43, Jan. 1963.

[23] R. Mittra and S. Laxpati, "Propagation in a wave guide with glide reflection symmetry," *Can. J. Phys.*, vol. 43, no. 2, pp. 353–372, 1965.

[24] R. Kieburtz and J. Impagliazzo, "Multimode propagation on radiating traveling-wave structures with glide-symmetric excitation," *IEEE Trans. Antennas Propag.*, vol. AP-18, no. 1, pp. 3–7, Jan. 1970.

[25] A. Hessel, M. H. Chen, R. C. M. Li, and A. A. Oliner, "Propagation in periodically loaded waveguides with higher symmetries," *Proc. IEEE*, vol. 61, no. 2, pp. 183–195, Feb. 1973.

[26] T. Chang *et al.*, "Broadband giant-refractive-index material based on mesoscopic space-filling curves," *Nature Commun.*, vol. 7, Aug. 2016, Art. no. 12661.

[27] D. Cavallo and C. Felita, "Analytical formulas for artificial dielectrics with nonaligned layers," *IEEE Trans. Antennas Propag.*, vol. 65, no. 10, pp. 5303–5311, Oct. 2017.

[28] P. Arnberg, O. B. Petersson, O. Zetterstrom, F. Ghasemifard, and O. Quevedo-Teruel, "High refractive index electromagnetic devices in printed technology based on glide-symmetric periodic structures," *Appl. Sci.*, vol. 10, no. 9, 2020, Art. no. 3216.

[29] M. Ebrahimpouri and O. Quevedo-Teruel, "Ultrawideband anisotropic glide-symmetric metasurfaces," *IEEE Antennas Wireless Propag. Lett.*, vol. 18, no. 8, pp. 1547–1551, Aug. 2019.

[30] A. Alex-Amor *et al.*, "Glide-symmetric metallic structures with elliptical holes for lens compression," *IEEE Trans. Microw. Theory Techn.*, vol. 68, no. 10, pp. 4236–4248, Oct. 2020.

[31] P. Bantavis, C. G. Gonzalez, R. Sauleau, G. Goussetis, S. Tubau, and H. Legay, "Broadband graded index Gutman lens with a wide field of view utilizing artificial dielectrics: A design methodology," *Opt. Express*, vol. 28, no. 10, pp. 14648–14 661, May 2020.

[32] W. Yuan *et al.*, "Glide-symmetric lens antenna in gap waveguide technology," *IEEE Trans. Antennas Propag.*, vol. 68, no. 4, pp. 2612–2620, Apr. 2020.

[33] G. Valerio, F. Ghasemifard, Z. Sipus, and O. Quevedo-Teruel, "Glide-symmetric all-metal holey metasurfaces for low-dispersive artificial materials: Modeling and properties," *IEEE Trans. Microw. Theory Techn.*, vol. 66, no. 7, pp. 3210–3223, Jul. 2018.

[34] Q. Chen, F. Mesa, P. Padilla, X. Yin, and O. Quevedo-Teruel, "Efficient leaky-lens antenna at 60 GHz based on a substrate-integrated-holey metasurface," *IEEE Trans. Antennas Propag.*, vol. 68, no. 12, pp. 7777–7784, Dec. 2020.

[35] M. Ebrahimpouri, O. Quevedo-Teruel, and E. Rajo-Iglesias, "Design guidelines for gap waveguide technology based on glide-symmetric holey structures," *IEEE Microw. Wireless Compon. Lett.*, vol. 27, no. 6, pp. 542–544, Jun. 2017.

[36] F. Ghasemifard, F. Mesa, G. Valerio, and O. Quevedo-Teruel, "Propagation characteristics in substrate integrated holey metasurfaces," in *Proc. 14th Eur. Conf. Antennas Propag.*, 2020, pp. 1–4.

[37] "CST Microwave Studio, version 2019." Accessed: Nov. 3, 2020. [Online]. Available: http://www.cst.com/